JOURNAL OF MAGNETIC RESONANCE **134,** 223–235 (1998)
ARTICLE NO. MN981510

Evolution Strategy Optimization for Selective Pulses in NMR

E. Lunati,* P. Cofrancesco,* M. Villa,*,[1] P. Marzola,† and F. Osculati†

*Unità INFM c/o Dipartmento di Fisica dell'Università, 27100 Pavia, Italy, and †Istituto di Anatomia e Istologia dell'Università, 37100 Verona, Italy

Received December 30, 1997; revised April 30, 1998

We present a first set of improved selective pulses, obtained with a numerical technique similar to the one proposed by Geen and Freeman. The novelty is essentially a robust and efficient "evolution strategy" which consistently leads, in a matter of minutes, to "solutions" better than those published so far. The other two ingredients are a "cost function," which includes contributions from peak and average radiofrequency power, and some understanding of the peculiar requirements of each type of pulse. For example, good solutions for self-refocusing pulses and "negative phase excitation pulses" (which yield a maximum signal well after the end of the pulse) are found, as may have been predicted, among amplitude modulated pulses with 270° tip angles. Emphasis is given to the search for solutions with low RF power for selective excitation, saturation, and inversion pulses. Experimental verification of accuracy and power requirements of the pulses has been performed with a 4.7 T Sisco imager.

Key Words: **selective-pulse design; optimization; evolution strategy; linear-phase pulses; power reduction.**

1. INTRODUCTION

Selective pulses are widely utilized in NMR imaging and high-resolution spectroscopy for perturbing the magnetization over a well-defined frequency range without affecting the magnetization elsewhere. They serve a range of purposes and should, correspondingly, satisfy different requirements. However, a major consideration in pulse design has always been the type of the hardware, which may or may not permit both phase and amplitude modulation of the RF excitation. For example, composite pulses exploit the coarse phase-shifting capability of the early spectrometers, and achieve efficient broadband decoupling or minimal sensitivity to RF inhomogeneities without resorting to amplitude modulation. A better solution of the uniform irradiation problem with inhomogeneous RF fields is offered by the adiabatic pulses, which requires complex (phase and amplitude) modulation, a standard feature in modern spectrometers. In the future, localized spectroscopy will deal with the problem of an RF excitation in the presence of rapidly varying, rather than static, magnetic gradients.

[1] To whom correspondence should be addressed at Dipartimento di Fisica "A. Volta," via Bassi, 6, I-27000 Pavia (Italy). Fax: +39 382 507221. E-mail: mvilla@matsci.unipv.it.

Even if relaxation is neglected, and gradients are static, a treatment of the spin-excitation problem outside the linear regime is not simple, since it belongs to the class of the so-called ill-posed, or inverse, problems for which an exact, or unique, "solution" does not exist. Several approximate analytical techniques have been developed: for instance, the Shinnar–Le Roux transform (*1, 2*) and the inverse scattering theory (*3*) find a solution for magnetization profiles which are approximated by polynomial or rational functions. Another approach involves numerical optimization of the pulse function described in a parameter space which, ideally, covers all allowed pulses. A search is made, in that space, for a "solution" which minimize a suitable error function, measuring the "distance" between target and properties of the actual pulse (*4*). A numerical approach of this kind is due to Geen and Freeman (*5*). In their method, the pulse "amplitude" (with sign) is written as a truncated Fourier series; the trajectory of each component of the magnetization during the pulse is followed by integration of the Bloch equations, the resulting magnetization profile is computed, and an "error" value is assigned to it, which is related with the rms difference relative to the ideal profile. The search for the optimal pulse is initially performed by repeating the previous steps many times with randomly chosen Fourier coefficients; the best solution found by the stochastic optimization is then refined through deterministic optimization.

We have found that a modified Geen and Freeman approach can be successfully applied, with proper care, to many types of selective excitation. The adiabatic and composite pulses are, in part, an exception, and will be discussed in a separate paper. With our algorithm, it takes, typically, a Pentium PC a few minutes to converge, from any starting point, to a solution of the problem which is, at least, as good as any other solution so far published. The key technical advance is a robust stochastic optimizer, with a "strategy" that automatically goes from "coarse search" to "refinement." As an example, Fig. 1 compares the magnetization profiles of the self-refocusing pulse (E-BURP2) of Geen and Freeman with our solution, obtained with 50,000 "attempts" (a little over 1 h with a Pentium). We have used the same Fourier expansion (10 harmonics) and the same error function as Geen and Freeman. Our deviations from ideality are substantially less than those of Geen and Freeman;

1090-7807/98 $25.00

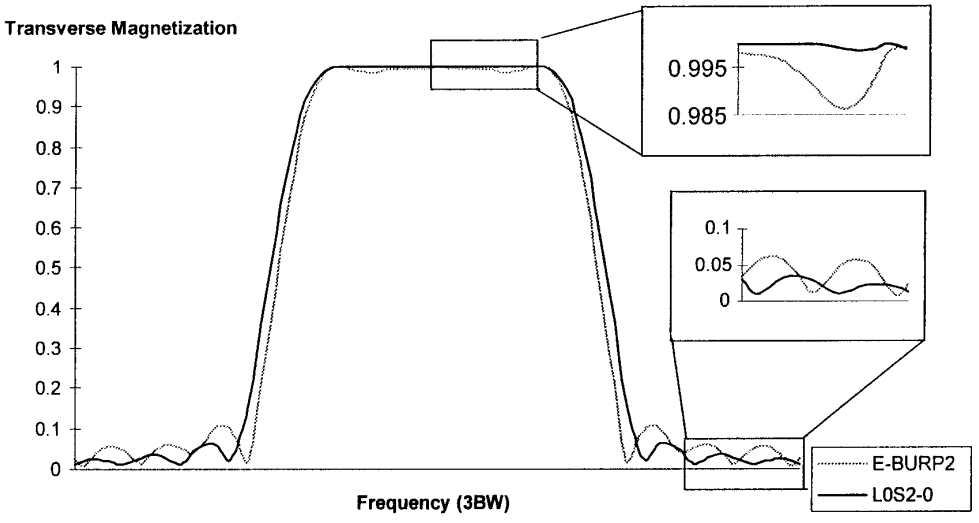

FIG. 1. Comparison between self-refocusing pulses E-BURP2 (Geen and Freeman) and L0S2-0 (new).

the rms error is 2.2% (against 4.3%), while peak power and average power of the two pulses are the same.

The goal of the article is to outline the procedures which constitute our method, and to present some of the optimized complex pulses which may be downloaded from our Web site (*6*). It will be apparent that, by substituting the error function with a

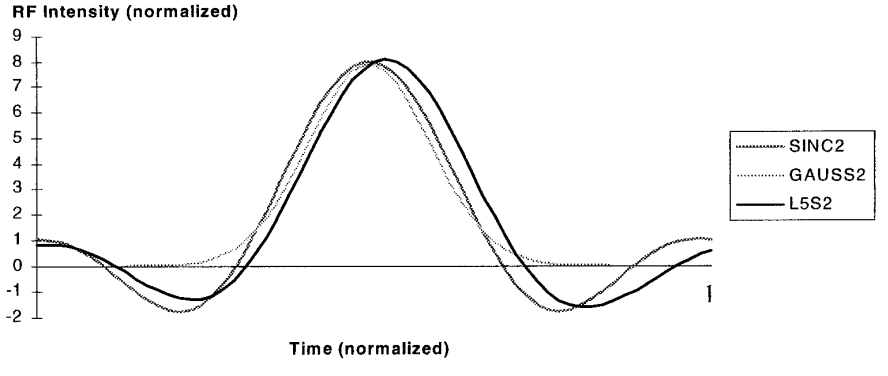

(a)

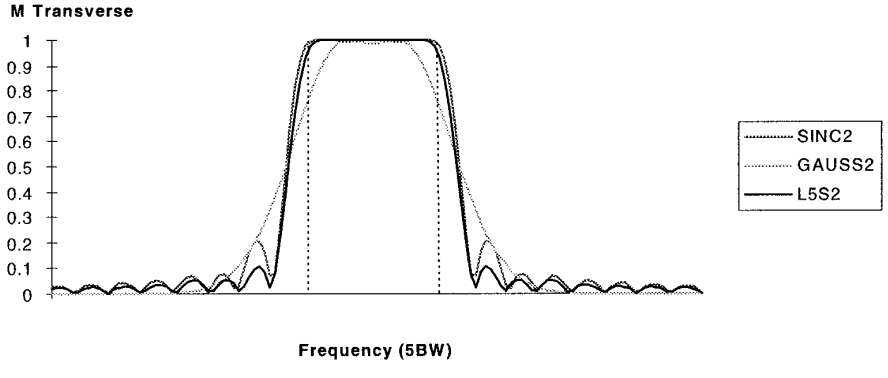

(b)

FIG. 2. Comparison of pulses with $k = +0.5$ $\sigma = 0.25$: the sinc and Gaussian pulses and the new L5S2. (a) Pulse shape; (b) transverse response.

TABLE 1
Comparison between New and Traditional Pulses

Pulse	Properties	N_P	σ	k	P_{pk}	P_m	$\sqrt{E}^b$(%)
L5S2	Excit. 90	9	0.25	+0.5	4.08	0.74	3.3
Sinc2	Excit. 90	2	0.25	+0.5	3.99	0.74	5.7
Gauss2	Excit. 90	2	0.25	+0.5	3.88	0.60	11.9
L5S5	Excit. 90	9	0.5	+0.5	3.52	1.26	9.2
Sinc5	Excit. 90	2	0.5	+0.5	3.78	1.32	10.2
Gauss5	Excit. 90	2	0.5	+0.5	3.79	1.38	11.7
L3S5	Excit. 90	15	0.5	+0.333	4.02	1.43	7.3
L0S2-0	Excit. 90	21	0.25	0	44.5	7.80	4.6
EBURP2[a]	Excit. 90	21	0.25	0	45.5	7.77	4.9
L0S2-1	Excit. 90	15	0.25	0	15.3	5.28	5.2
EBURP1[a]	Excit. 90	17	0.25	0	28.6	5.87	4.9
L0S3	Excit. 90	11	0.333	0	27.1	5.33	9.9
L0S5	Excit. 90	9	0.5	0	33.8	9.49	12.3
L-5S2	Excit. 90	13	0.25	−0.5	21.7	4.02	11.2
L-3S4	Excit. 90	19	0.4	−0.333	27.0	7.85	9.3
SAS2	Satur. 90	9	0.25		3.68	0.73	3.0
INS2	Inver. 180	15	0.25		16.1	5.43	9.0
I-BURP1[a]	Inver. 180	19	0.25		27.4	6.62	11.0
I-BURP2[a]	Inver. 180	23	0.25		61.4	6.80	11.5
RES2	Refoc. 180	12	0.25		57.3	6.37	17.0
RE-BURP[a]	Refoc. 180	16	0.25		92.7	7.76	17.2

[a] From Geen and Freeman (*5*).
[b] All errors are computed with a transition band $\beta = \frac{1}{6}$.

more general "cost" function, it is very easy to accommodate different kinds of constraints, and compromise between reduced RF power and accuracy of the profile. Sometimes, we drastically changed the number of parameters (or harmonics) and found empirically what we should have known from the outset: In some cases, phase modulation is really not needed; adding parameters beyond a certain limit reduces the quality of the solution which is found with a given number of iterations.

2. METHODS

As hinted in the Introduction, a numerical approach to the selective excitation problem comprises the following elements:

1. *Pulse shape parametrization.* While phase and amplitude modulations are applied and computed in a stepwise fashion, it is usually convenient to deal with analytic forms of these modulations which have some smoothness. If the time step is substantially shorter than the reciprocal bandwidth of the NMR signal, the discrete nature of the excitation should become irrelevant. The argument may not be so clear-cut when we consider a variable magnetic gradient, or field, as a part of the excitation (Tannus and Garwood (*7*)), but it should essentially hold with static fields. An implication is that a "soft" upper limit exists for the number of harmonics which may reasonably be taken into account. In the following, the pulse length is divided into 64 time steps and the time functions are, typically, expanded in a Fourier series with up to 20 harmonics.

2. We define the ideal *target function* with the desired M_x, M_y, M_z profiles, and a rule to compute the *error function,* a measure of the "distance" between the calculated magnetization profiles and the target function. We also introduce a *cost function,* which is linearly related with the error function and may include the peak and/or the average pulse power. By handling this cost function rather than the error function, we may automatically avoid solutions with excessive deposited power, or which are not compatible with the RF amplifiers. We may also compromise between low power and small error.

3. We choose an *optimization strategy,* which leads to a "solution," i.e. to identify a pulse with minimal "cost."

Parametrization and Computation

We are not suggesting a "black box" solution of the selective pulses problem: On the contrary, we found it very important to translate our understanding of the problem into the choices which lead to the parametrization of the pulse, particularly for adiabatic and composite pulses. We refuse the brute force approach of a "point-by-point" pulse definition for the same reasons as Geen and Freeman, which are theoretical (functions should be "smooth") and practical

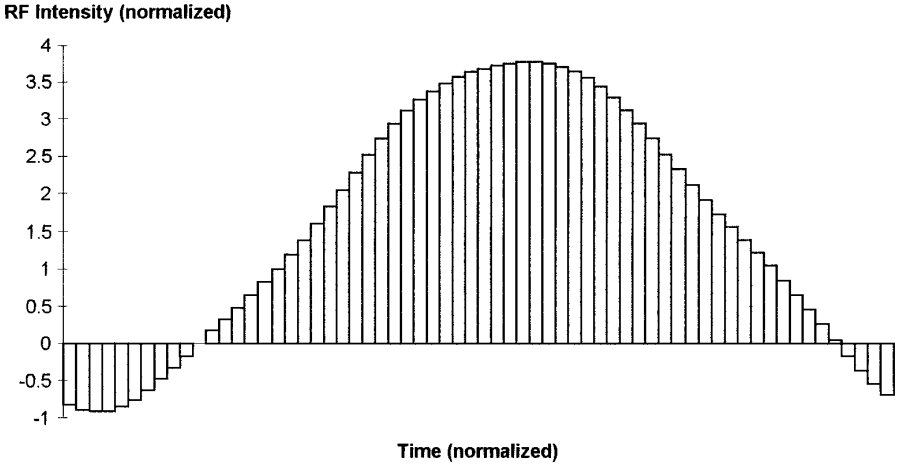

(a)

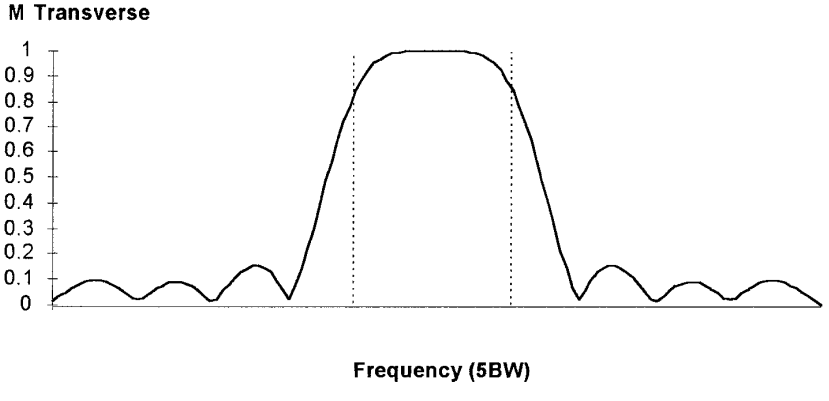

(b)

FIG. 3. Shape profile (a) and transverse response (b) of pulse L5S5 ($k = 0.5$, $\sigma = 0.5$).

(optimization may be very difficult and long in a high-dimension parameter space). A Fourier series approach satisfies these requirements; we have used it both for amplitude modulation (as Geen and Freeman did), and for complex modulation (phase and amplitude) which will be presented here because more general. We have also attempted other types of expansion proposed in the literature (*8*, *9*), but found no advantage in them.

We will use time and frequencies normalized with the pulse duration T_p:

$$\tau = t/T_p;\ w = \omega T_p. \qquad [1]$$

Amplitude and phase modulation are defined through the real and imaginary components w_{1x} and w_{1y}, written as

$$w_{1x}(\tau) = 2\pi\{\sum_{n=0}^{N_p} [A_n\cos(2\pi n\tau) + B_n\sin(2\pi n\tau)]\} \qquad [2a]$$

$$w_{1y}(\tau) = 2\pi\{\sum_{n=0}^{N_p} [C_n\cos(2\pi n\tau) + D_n\sin(2\pi n\tau)]\}, \qquad [2b]$$

where $A_n \ldots D_n$ are the optimization parameters and N_p should be substantially smaller than the number N of steps. Neglecting relaxation, we can obtain the final magnetization profile ($\tau = 1$), by orderly multiplying the Bloch rotation matrices R_n of each step

$$\mathbf{M}(1) = \prod_{n=1}^{N} R_n\mathbf{M}(0). \qquad [3]$$

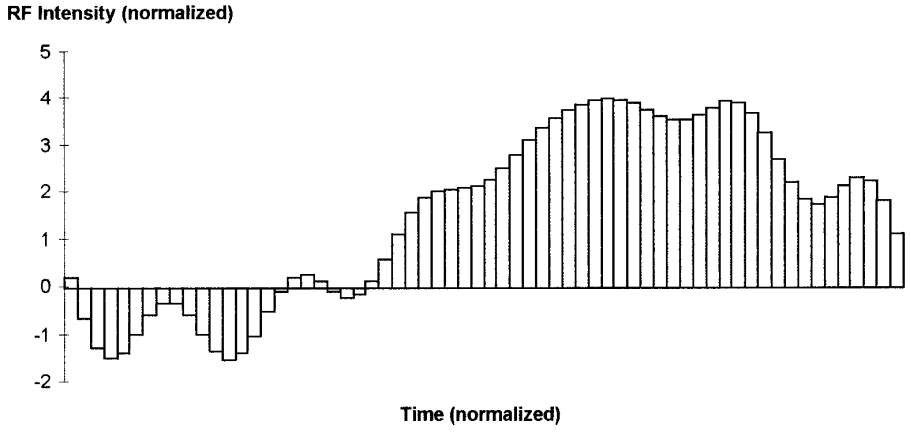

(a)

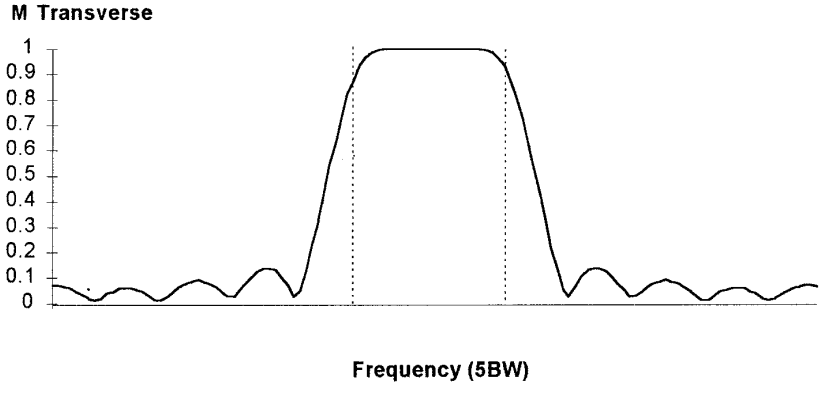

(b)

FIG. 4. Shape profile (a) and transverse response (b) of pulse L3S5 ($k = 0.333$, $\sigma = 0.5$).

Here $\mathbf{M}(0)$ is the starting magnetization vector, and

$$R_n = \begin{pmatrix} R_{xx} & R_1 + R_2 & R_3 - R_4 \\ R_1 - R_2 & R_{yy} & R_5 + R_6 \\ R_3 + R_4 & R_5 - R_6 & R_{zz} \end{pmatrix}, \quad [4]$$

with

$$R_{xx} = \cos^2\phi_n(\cos^2\theta_n\cos\rho_n + \sin^2\theta_n) + \sin^2\phi_n\cos\rho_n \quad [5a]$$

$$R_{yy} = \sin^2\phi_n(\cos^2\theta_n\cos\rho_n + \sin^2\theta_n) + \cos^2\phi_n\cos\rho_n \quad [5b]$$

$$R_{zz} = \sin^2\theta_n\cos\rho_n + \cos^2\theta_n \quad [5c]$$

$$R_1 = \sin\phi_n\cos\phi_n\sin^2\theta_n(1 - \cos\rho_n) \quad [5d]$$

$$R_2 = \cos\theta_n\sin\rho_n \quad [5e]$$

$$R_3 = \cos\phi_n\sin\theta_n\cos\theta_n(1 - \cos\rho_n) \quad [5f]$$

$$R_4 = \sin\phi_n\sin\theta_n\sin\rho_n \quad [5g]$$

$$R_5 = \sin\phi_n\sin\theta_n\cos\theta_n(1 - \cos\rho_n) \quad [5h]$$

$$R_6 = \cos\phi_n\sin\theta_n\sin\rho_n. \quad [5i]$$

In these equations, ρ_n, ϕ_n, θ_n refer to the nth step and are, respectively, the precession angle around $\mathbf{B}_{eff}$ (the effective field), the phase of $\mathbf{B}_{eff}$ in the xy plane, and the tilt of $\mathbf{B}_{eff}$ from the z axis.

The vector $\mathbf{B}_{eff}$ depends on the offset (normalized) Δw: For any pulse shape, the Bloch equations algorithm provides the final magnetization vs the offset, i.e., the *response function* $\mathbf{M}(\Delta w)$, which should be compared with the *target function* $\mathbf{M}^T(\Delta w)$. Following Geen and Freeman we introduce the *selectivity* σ as

$$\sigma = \frac{1}{BW \cdot T_P}, \quad [6]$$

where BW is the desired bandwidth in hertz. It follows that the

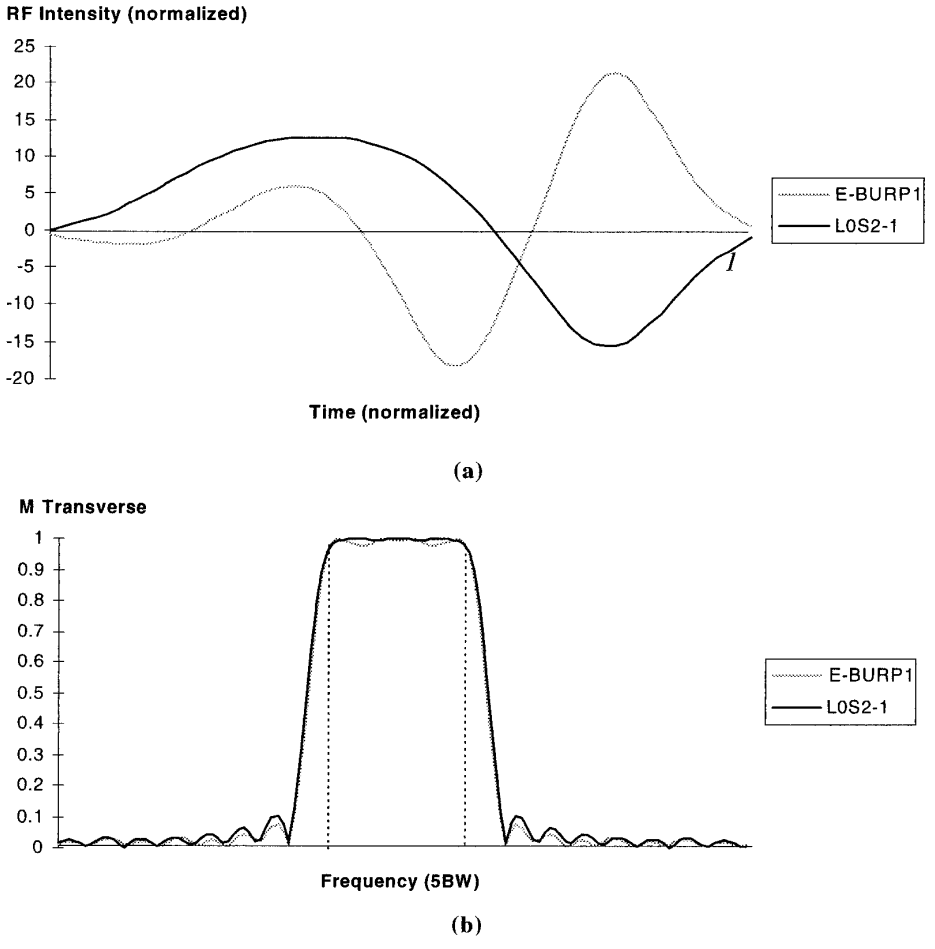

FIG. 5. Comparison of self-refocusing pulses ($k = 0$) with $\sigma = 0.25$: E-BURP1 (Geen and Freeman) and L0S2-1 (new). (a) Pulse shape; (b) transverse response.

normalized bandwidth $w_{in} \equiv 2\pi BW \cdot T_P$ and selectivity are simply related:

$$w_{in} = \frac{2\pi}{\sigma}. \qquad [7]$$

The Cost Function

It seems natural to accept that the response to a selective pulse will always exhibit a transition band, which cannot be extremely narrow. It also makes sense not to impose any prescription for the behavior of the magnetization in this band; in a similar way, an engineer specifies a filter by giving cutoff frequencies, maximum in-band oscillation, minimum off-band attenuation, and extension of the transition regions. We will consider the following band regions:

$$\text{“}in\text{”}: |w| \le \frac{w_{in}}{2} \qquad [8a]$$

$$\text{“}trans\text{”}: \frac{w_{in}}{2} < |w| \le w_{in}\left(\frac{1}{2} + \beta\right) \qquad [8b]$$

$$\text{“}out\text{”}: w_{in}\left(\frac{1}{2} + \beta\right) < |w| \le w_{max}. \qquad [8c]$$

The error function $E\{x_i\}$ will be defined as combination of mean square deviations within the in-band and out-of-band regions, for all three components of the magnetization. If (x_i) is a point in the parameter space, we set

$$E\{x_i\} = \sum_{\alpha} X_\alpha^2, \qquad [9]$$

where $\alpha = x, y, z$ and

$$X_\alpha^2\{x_i\} = \frac{\zeta_\alpha^{in} \sum_{k \in in} [M_\alpha(\Delta w_k, \{x_i\}) - M_\alpha^T(\Delta w_k)]^2 + \zeta_\alpha^{out} \sum_{k \in out} [M_\alpha(\Delta w_k, \{x_i\}) - M_\alpha^T(\Delta w_k)]^2}{\zeta_\alpha^{in} N_{in} + \zeta_\alpha^{out} N_{out}} \qquad [10]$$

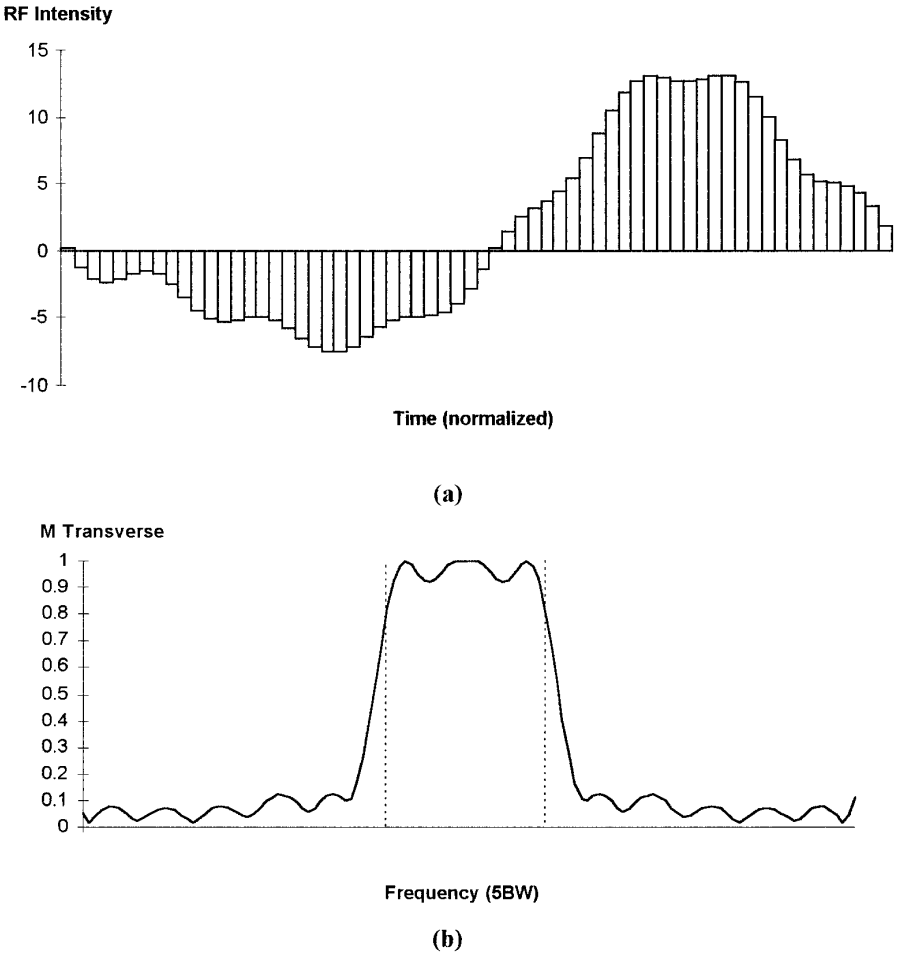

FIG. 6. Shape profile (a) and transverse response (b) of pulse L-3S4 ($k = -0.333$, $\sigma = 0.4$).

and $N_{in}N_{out}$ are the number of frequency points in-band and out-of-band, respectively. Notice that we may give different relative weights ζ to components of the magnetization and to band regions. In the following, we will always set $\zeta_x = \zeta_y$.

To take RF power into consideration, we begin noticing that it scales as T_P^{-1}, i.e., the ratio between power W and bandwidth squared $(BW)^2$ does not depend upon pulse duration. Therefore, we introduce the *normalized power* as

$$p(\tau) = \sigma^2|\mathbf{w}_1(\tau)|^2 \propto \frac{W(\tau)}{BW^2}. \qquad [11]$$

and peak (p_{pk}) and mean (p_m) power as

$$p_{pk} = \sigma^2 MAX_{\{n\}}[|\mathbf{w}_1(\tau_n)|^2] \qquad [12a]$$

$$p_m = \frac{\sigma^2}{N}\sum_{n=1}^{N}|\mathbf{w}_1(\tau_n)|^2. \qquad [12b]$$

We define the cost function as

$$E_c\{x_i\} = \sum_{\alpha} X_\alpha^2 + \lambda_1 p_{pk} + \lambda_2 p_m, \qquad [13]$$

where the λ_1, λ_2 coefficients are carefully set, during the optimization of each pulse, according to the relative magnitudes of the response profile error, p_{pk} and p_m, and in view of the performances required to each solution. Alternatively, we may have controlled the RF power by setting an upper limit to p_{pk} or p_m (*10*) and neglecting all solution beyond these limits. However, we found it more instructive always to search for a power efficient pulse, with the exception of the case presented in Fig. 1, where our purpose was to compare optimization strategies.

Optimization Strategy

The cost function $E_c\{x_i\}$ must be minimized in a space $\{x_i\}$, which has up to 50 parameters constrained by condi-

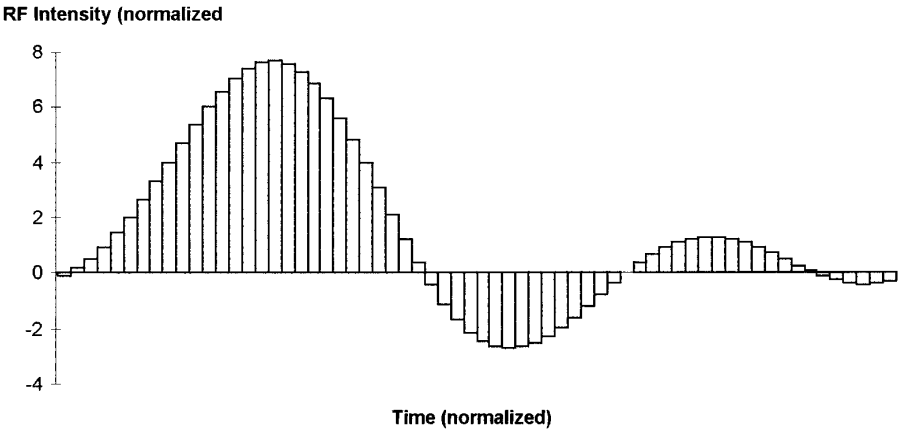

(a)

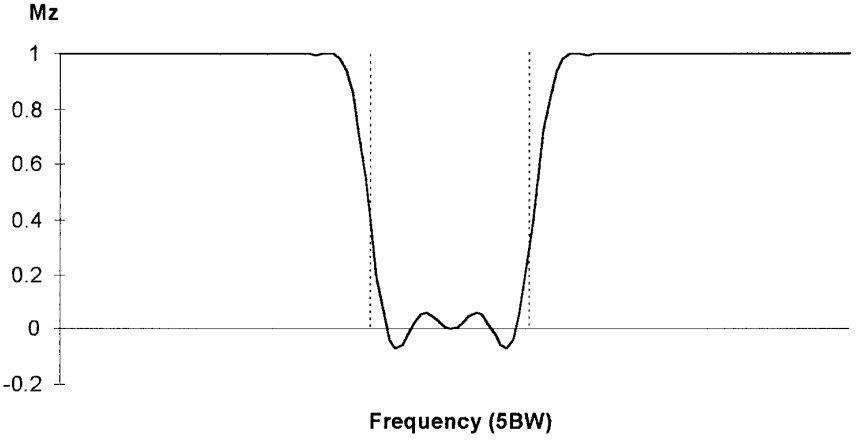

(b)

FIG. 7. Shape profile (a) and M_z response (b) of the saturation pulse SAS2 ($\sigma = 0.25$).

tions of the type $u_i < x_i < v_i$. The *deterministic* optimizers build a sequence of solutions $\mathbf{x}^{(m)}$ with the recursive equation

$$\mathbf{x}^{(m+1)} = \mathbf{x}^{(m)} + a^{(m)}\mathbf{s}^{(m)}, \qquad [14]$$

beginning with an initial guess $\mathbf{x}^{(0)}$. Here m is the iteration index, $a^{(m)}$ is called the *step*, and $\mathbf{s}^{(m)}$ the *slope*. Different choices of the slope vector $\mathbf{s}$ characterize the various methods; for example, if we move our point in the direction of the fastest decrease of E, i.e.,

$$\mathbf{s}^{(m)} = -\text{grad}\, E(\mathbf{x}^{(m)}), \qquad [15]$$

we have the well-known *steepest descent* method. All popular choices of the slope $\mathbf{s}$ (i.e., quasi-Newton, conjugate gradient) involve a finite-difference estimation of the derivatives of the error function $E(\mathbf{x}^{(m)})$. All these methods may be grouped together in the large class of the so-called higher order deterministic optimization methods (HODOM).

However, when the dimension of the parameter space increases, the cost function is likely to have many local minima, and each of them may trap the trajectory of points $x^{(m)}$. In this case, *stochastic* methods are usually more effective. Even if they have common mathematical foundations (*11*), the stochastic algorithms take different names (simulated annealing (*12, 13*), genetic (*14, 15*), evolution strategies (*16*), . . .), but may be collectively called zeroth-order stochastic optimization methods (ZOSOM). We begin the mth iteration with a set of μ "parent" vectors: $\mathbf{x}_1^{(m)}, \ldots, \mathbf{x}_\mu^{(m)}$; from these, λ "children" vectors $\mathbf{y}_1^{(m)}, \ldots, \mathbf{y}_\lambda^{(m)}$ are generated according to the probability law

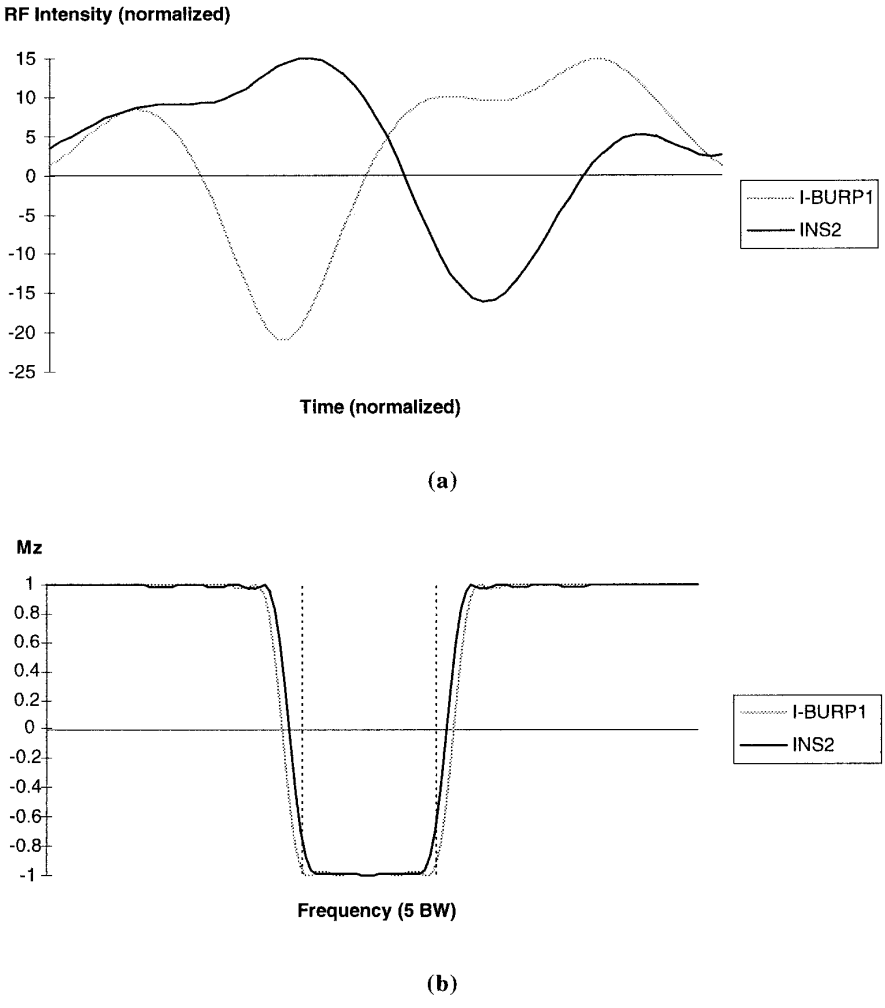

FIG. 8. Comparison of inversion pulses with $\sigma = 0.25$: I-BURP1 (Geen and Freeman) and INS2 (new). (a) Pulse shape; (b) M_z response.

$$\rho(\mathbf{y}, \langle \mathbf{x} \rangle_\mu, \mathbf{d}) = \exp\left[-\sum_i \left(\frac{y_i - \langle x_i \rangle_\mu}{d_i} \right)^2 \right], \qquad [16]$$

where ρ is the probability density, $\langle x_i \rangle$ is the average of the ith parameter over the parents, and $\mathbf{d} = \{d_i\}$ is a dispersion vector, adjusted at each iteration. We have a $(\mu + \lambda)$ strategy if in the next iteration the new parents are the μ vectors with the smallest errors in the set comprising both parents and children. We have a (μ, λ) strategy if $\lambda > \mu$ and the best μ vectors are selected among the children only. The main feature of an *evolution strategy* (*17*) is the rule by which the dispersion is modified. When the parents are close to the minimum and the range of search is much larger than the distance from it, very few of the children will be better than the parents, and the value of $\|\mathbf{d}\|$ should be reduced; when children are frequently better than parents, the dispersion should be increased, to explore regions farther away from $\langle \mathbf{x} \rangle$. A decision about the dispersion of the next step should be taken on the basis of a statistically significant number of generations. The tuning elements of the evolution strategy are the length of the "history" upon which the statistic is made, the dispersion fractional change, and the critical success rate of children that triggers an increase of the search range. When we increase the number of parameters, we need to increase the evolution history, but total computation time, in principle, is almost unaffected.

The stochastic methods have several distinct advantages relative to the deterministic methods. First, they are more effective in reaching a global minimum, or at least a very stable local minimum. Second, they are more robust, since oscillating trajectories are avoided. Third, no assumptions have to be made about the smoothness of the cost function, as required during the computation of the derivatives. And last, the treatment of constraint conditions is usually much simpler than in HODOMs. Among the stochastic algorithms an evolution optimizer is preferable to the simulated anneal-

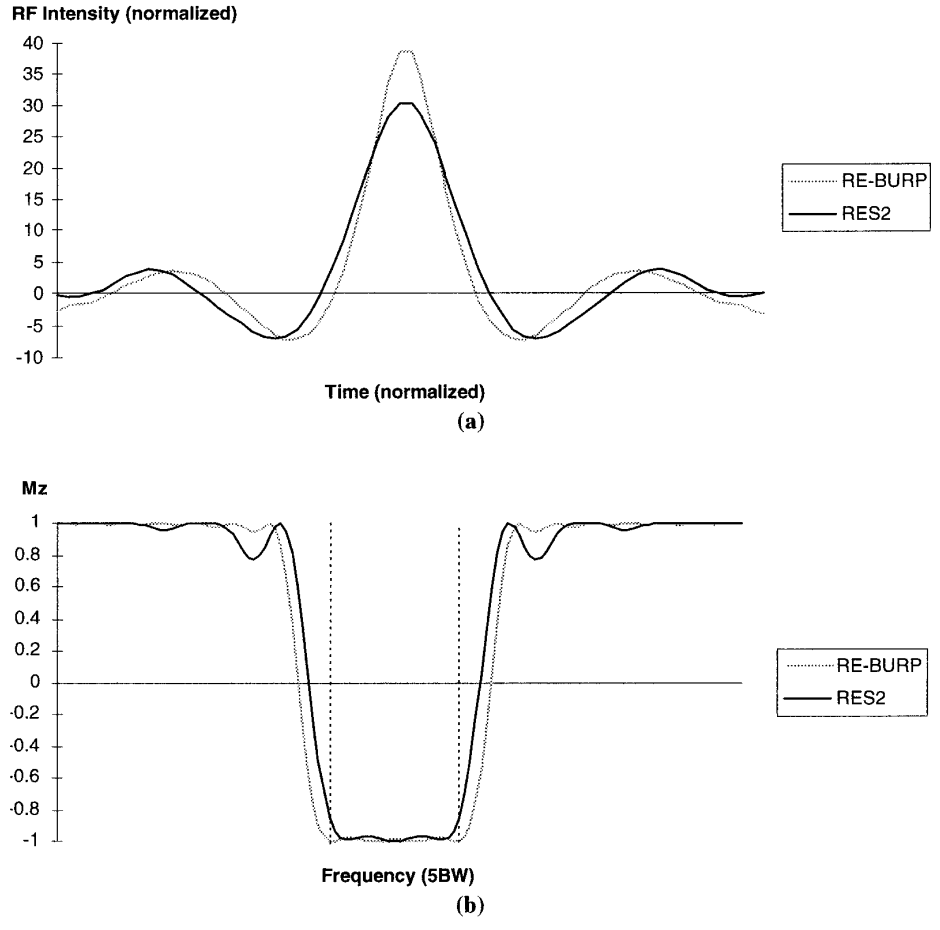

FIG. 9. Comparison of refocusing pulses with $\sigma = 0.25$: RE-BURP (Geen and Freeman) and RES2 (new). (a) Pulse shape; (b) M_z response.

ing of Geen and Freeman because it can approach the minimum with no need for deterministic refinement. We will use an evolution strategy carefully tailored to the selective excitation problem, which regularly yields a "good" solution in a few hundred iterations.

3. RESULTS

Linear-Phase Selective 90° Pulses

The problem is to find a selective, 90° pulse in which the response phase is proportional to the frequency offset (linear-phase pulses (*18*)): $\varphi = k\Delta w$. The constant of proportionality k may be positive, as for ordinary pulses, negative, as for the "prefocused pulses" of Ngo and Morris (*19*), or zero, as for the so-called self-refocusing pulses (*5, 20, 21*). In unit of M_0, the equilibrium magnetization value, the target function is (see Eqs. [8])

$$M_x^T(\Delta w) = \sin(k\Delta w) \quad [17a]$$

$$M_x^T(\Delta w) = \cos(k\Delta w) \quad [17b]$$

$$M_z^T(\Delta w) = 0 \quad [17c]$$

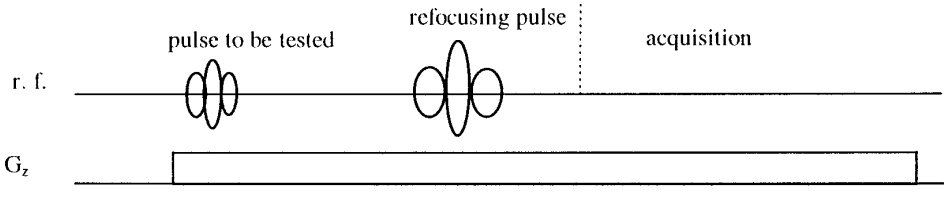

FIG. 10. Sequence for acquisition of 90° pulse response.

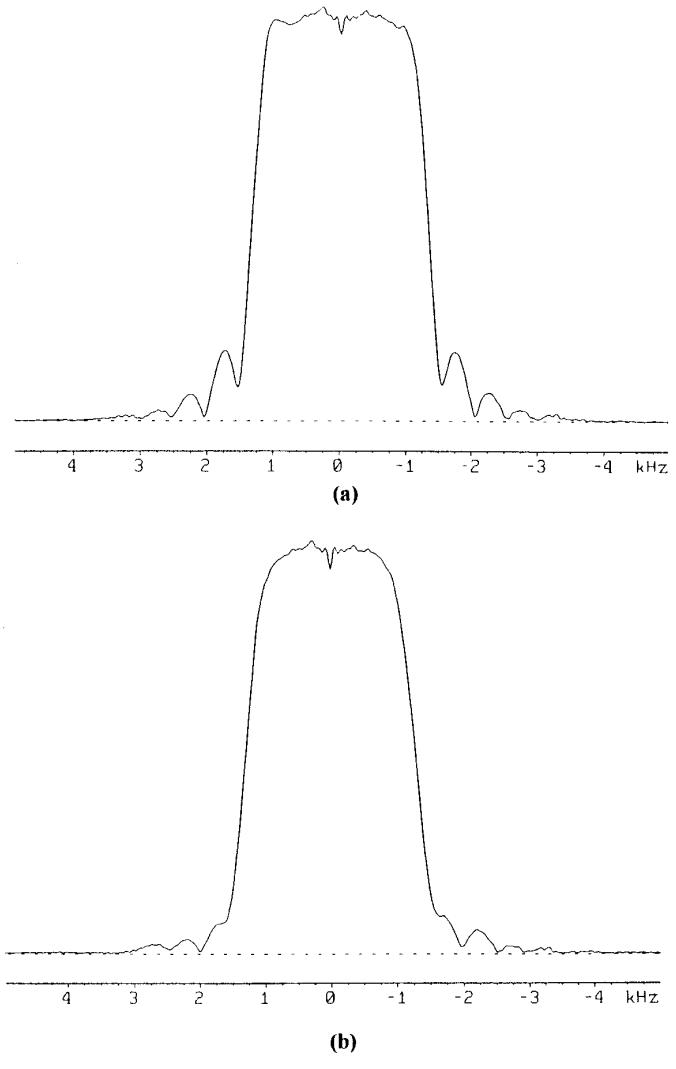

FIG. 11. Response of (a) sinc (+38 dB) and (b) L5S2 (+37 dB) pulses.

when $|\Delta w| \leq w_{in}/2$, while

$$M_x^T(\Delta w) = 0 \qquad [18a]$$

$$M_y^T(\Delta w) = 0 \qquad [18b]$$

$$M_z^T(\Delta w) = 1 \qquad [18c]$$

when $w_{in}/2 < |\Delta w| \leq w_{max}$. When the coefficient k is positive, refocusing is usually accomplished with an inverted gradient in MRI and/or with a hard 180° pulse. When k is negative, the maximum signal is achieved sometimes after the pulse end, with no change in $\mathbf{B}_0$. When $k = 0$, all signal components are in phase when the pulse ends.

Positive phase is a "natural" feature of excitation pulses. In fact, the linear response theory provides, as the best selective pulse shape, the sinc function, which gives a coefficient $k = 0.5$; in imaging we then need to invert the gradient for a time $0.5\ T_P$ to obtain an echo. A Gaussian pulse also has $k = 0.5$. When we search for amplitude and phase modulated solutions with $k = 0.5$, the algorithm spontaneously converges toward real (purely AM) pulses, similar to slightly shifted sinc shapes; correspondingly, the response is symmetric around the center frequency. Figure 2 compares a sinc and a Gauss pulse (selectivity $\sigma = 0.25$) with our solution L5S2 (linear-phase pulse with $k = 0.5$ and selectivity = 0.25; see Table 1). These three pulses require essentially the same peak power, but the new one displays a better in-band profile than the Gauss and a better out-of-band profile than the sinc. With increasing selectivity (i.e., reduced time needed to excite the same bandwidth), the advantages of our solution L5S5 ($\sigma = 0.5$), relative to the corresponding Gauss and sinc pulses, becomes more evident, as reported in the table; this pulse is shown in Fig. 3. An interesting solution, which has no classical counterpart, is L3S5 ($k = 0.333$, $\sigma = 0.5$), which is shown in Fig. 4. With an inverted gradient, it requires only a $0.333\ T_P$ refocusing time, and uses the same power as a Gauss pulse.

Pulses with $k = 0$ are called *self-refocusing* pulses; the most commonly used are BURP (*5*) and SNEEZE pulses (*20, 21*). Geen and Freeman's E-BURP2 is a self-refocusing pulse with $\sigma = 0.25$, obtained via simulated annealing followed by deterministic refinement. It has been compared with our solution L0S2-0 (pulse with $k = 0$ and $\sigma = 0.25$, version 0), obtained with the same error function and selectivity of these authors, in Fig. 1. Notice from Table 1 that these two solutions require RF peak power p_{pk} of about 45, i.e., 10 times that of a Gaussian pulse. In the computation of Table 1 we adopted a narrower transition band than Geen and Freeman did ($\beta = \frac{1}{6}$ rather than $\beta = \frac{1}{4}$), and we routinely included peak and average power in our cost function. Results for the self-refocusing pulses are presented in Fig. 5, which compares the theoretical profiles of

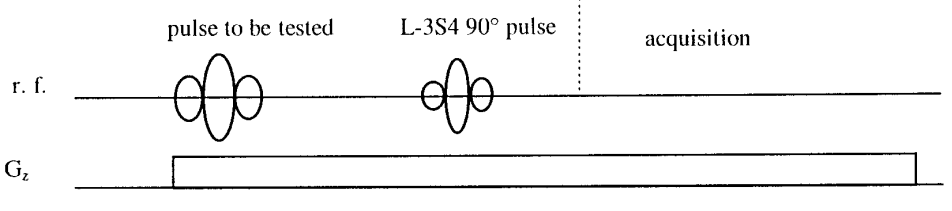

FIG. 12. Sequence for acquisition of 180° pulse response.

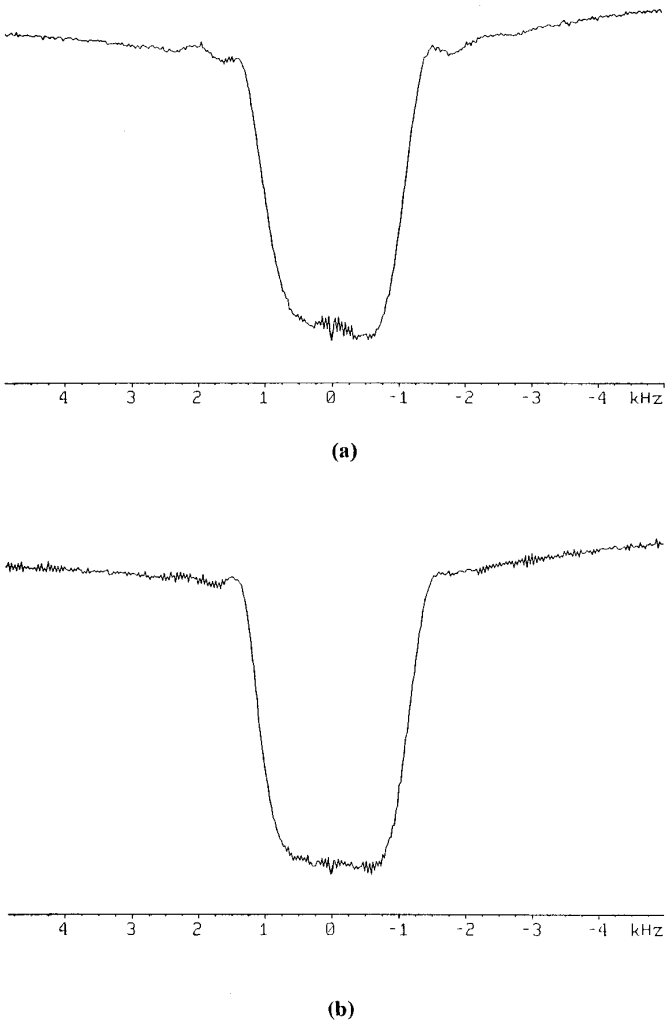

FIG. 13. Response of (a) I-BURP1 (+47 dB) and (b) INS2 (+44 dB) pulses.

Geen and Freeman's E-BURP1 pulse ($p_{pk} = 28.6$) with our low-power solution L0S2-1 ($p_{pk} = 15.3$). Our response is slightly worse, but we need half the peak power of E-BURP1 and one-third that of E-BURP2. In the table, we mention two self-refocusing 270° pulses: L0S3 ($\sigma = 0.333$) and L0S5 ($\sigma = 0.5$). Despite the higher tip angle, they require the same peak power as E-BURP1 while having higher selectivity and better phase behavior, as noted earlier by Emsley and Bodenhausen (*22*) when comparing Gaussian pulses of 90° and 270°. By the way, the optimization found these solutions by itself when no constraint was set on the pulse angle.

We found it quite difficult to generate good-looking and low power pulses with negative k: Response profiles are worse, and power much higher, than for positive pulses. In Table 1 we list several solutions: with $k = -0.5$, $\sigma = 0.25$ (L-5S2, a 270° pulse) or $k = -0.333$, $\sigma = 0.4$ (L-3S4). Figure 6 shows the pulse shape of L-3S4 and its response.

Saturation, Inversion and Refocusing Pulses

In addition to linear-phase pulses, MRI and NMR may need *saturation* pulses, *inversion* (or 180°) pulses, and *refocusing* pulses, all of which may be either hard or frequency-selective. The difference between linear-phase and saturation pulses is that, with the former, we are not interested in the phase of the in-plane magnetization: correspondingly, we may put $\gamma_x^{in} = \gamma_y^{in} = 0$ in Eq. [10]. They usually show better profile and power performances than the linear-phase pulses, because they are less constrained. Figure 7 shows the M_z magnetization profile of the saturation pulse SAS2 ($\sigma = 0.25$) which has smaller peak and mean power than the "natural" L5S2 linear-phase pulse.

Obviously, in-plane magnetization is ignored also in inversion pulses, which ideally have $M_z = -1$ in-band, and $M_z = 1$ elsewhere. Figure 8 compares I-BURP1 of Geen and Freeman ($p_{pk} = 27.4$) with our corresponding solution INS2 ($p_{pk} = 16.1$), both with $\sigma = 0.25$. Notice that our profile is sharper (this follows from using narrower transition bands than Freeman) and peak power smaller. For comparison, in the table we quote also the characteristics of I-BURP2, which needs more power than I-BURP1. As discussed by Geen and Freeman, a refocusing pulse should be time-symmetrical, and a real modulation with only cosine terms ($B_n = 0$, $D_n = 0$ in Eqs. [2]) will do. Our solution, found in this way (RES2) is compared with RE-BURP of Freeman in Fig. 9 and in the table. Our pulse is sharper, has worse off-band behavior, and requires nearly half peak power.

4. CONCLUSIONS

We have proposed a robust method to explore the spaces of solutions of band-selective pulses which seems to us superior to analytical or numerical approaches so far published. In particular, we consistently find low-power solutions by weighting the power in the cost function. We have discussed pulses with negative k which may find a variety of applications, e.g., in fast projection–reconstruction sequences.

5. EXPERIMENTAL

We tested our pulses with a Sisco-Varian 4.7 T imager and a cylindrical water phantom with axis along $\mathbf{B}_0$. We found that artifacts may be minimized, and sequence time reduced, by entirely avoiding gradient switching. The excitation bandwidth of the pulse to be tested was set to 2 kHz. Figure 10 shows the sequence employed to test linear-phase pulses. We used our refocusing pulse RES2 (independently tested) with a wider bandwidth (4 kHz) in order not to interfere with the profile of the first pulse. This setup allows one to measure the k value of the linear-phase pulses in terms of the time-shift of the echo obtained. We found delays consistent with our predictions, but

in Fig. 11 we show the absolute magnitude of the FT of the entire echo, which does not depend upon the echo time. The amplitude of the first pulse is tuned for maximum signal, and the reading of the attenuator yields a rough indication of the pulse power. Figure 11 compares the response of a sinc pulse ($\sigma = 0.25$) with the response of our L5S2; as expected, the last is better and requires about the same power (+37 dB for L5S2 and +38 dB for the sinc).

For inversion and saturation pulses we used the sequence of Fig. 12 with a very broadband (12.5 kHz) pulse with negative k L-3S2, 200 μs long, which allows acquisition to begin well after the dead time. Figure 13 compares INS2 with I-BURP1. Differences in shape are not significant (as expected), but INS2 needs amplification of +44 dB while I-BURP1 needs +47 dB in experiments with the same bandwidth.

REFERENCES

1. S. M. Eleff, V. H. Subramanian, M. Shinnar, S. Renn, and J. S. Leigh, *J. Magn. Reson.* **72,** 298 (1987).
2. J. Pauly, P. Le Roux, D. Nishimura, and A. Macovski, *IEEE Trans. Med. Imaging* **10,** 1 (1991).
3. J. W. Carlson, *J. Magn. Reson.* **94,** 376 (1991).
4. W. S. Warren and M. S. Silver, *Adv. Magn. Reson.* **12,** 247 (1988).
5. H. Geen and R. Freeman, *J. Magn. Reson.* **93,** 93 (1991).
6. http://matsci.unipv.it/persons/lunati/pulses.htm
7. A. Tannus and M. Garwood, *SMR Book of Abstracts,* 1543 (1997).
8. Z. Starcuk, Jr., K. Bartusek, and Z. Starcuk, *J. Magn. Reson. A* **106,** 106 (1994).
9. J. Slotboom, J. W. Gunning, A. F. Mehlkope, and W. M. J. J. Bovée, *J. Magn. Reson. A* **101,** 257 (1993).
10. S. Topp and K. Schaumburg, *SMR Book of Abstracts,* 1457 (1996).
11. A. Gottvald, K. Preis, C. Magele, O. Biro, and A. Savini, *IEEE Trans. Magn.* **28,** 3 (1992).
12. S. Kirkpatrick, C. D. Gelatt, and M. P. Vecchi, *Science* **220,** 671 (1983).
13. I. O. Bohachevsky, M. E. Johnson, and M. L. Stein, *Technometrics* **28,** 209 (1986).
14. L. Davis, "Genetic Algorithms and Simulated Annealing," Morgan Kauffmann Publishers, Los Altos (1989).
15. X. Wu and R. Freeman, *J. Magn. Reson.* **85,** 414 (1989).
16. A. Gottvald, K. Preis, and M. Friedrich, *IGTE Symposium,* Graz, p. 23 (1990).
17. P. Cofrancesco, S. Scotti, M. Villa, P. Mustarelli, and A. Gottvald, *Solid State Ionics* **53–56,** 868 (1992).
18. M. Villa, P. Cofrancesco, A. Gottvald, A. Boicelli, and U. Guerrini, *SMR Book of Abstracts,* 124 (1994).
19. J. T. Ngo and P. J. Morris, *Magn. Reson. Med.* **5,** 217 (1987).
20. J.-M. Nuzillard and R. Freeman, *J. Magn. Reson. A* **110,** 252 (1994).
21. Ē. Kupče and R. Freeman, *J. Magn. Reson. A* **112,** 134 (1995).
22. L. Emsley and G. Bodenhausen, *J. Magn. Reson.* **82,** 211 (1989).